Powder Flow Testing with 2D and 3D Biaxial and Triaxial simulations

C. T. David, R. García-Rojo, H. J. Herrmann, S. Luding (*)
Institute of Computer Physics, Univ. of Stuttgart, Pfaffenwaldring, 27, 70569 Stuttgart, Germany
(*) Particle Technology, Nanostructured Materials, DelftChemTech, TUDelft, Julianalaan 136, 2628 BL Delft, The Netherlands, e-mail: s.luding@tudelft.nl

This paper is dedicated to late Prof. Brian Scarlett

ABSTRACT

The mechanical response of frictional powders under quasi-static loading is studied by means of two- and three-dimensional discrete element methods, compared directly with each other. The response of the system is characterized by elastic behavior for very small deformations, softening, plastic yield and critical state flow at large strain. The maximal yield stress is reached for some finite deformation of a few percent, but the decay to the critical steady state flow regime is much slower in the 3D situation than in the 2D systems examined here. The critical state regime is thus reached much later and at considerably higher dilation level in 3D. Possible reasons for this qualitative difference are discussed but more studies are needed to identify them properly.

KEYWORDS: Particle simulation, friction, creep, critical state flow

I. INTRODUCTION

Elementary powder tests, see Ref. [11,13] and references therein, are a straightforward way to determine empirical laws and to determine the parameters for constitutive laws. One possibility to perform these experiments is the bi- or tri-axial setup, see Ref. [12] and references therein, where the system is confined in a cuboid container and the powder is subject to slow, quasi-static deformations, different in two or three directions, respectively. The deformations can be performed in a single sweep or periodically, over many cycles [2,10] in order to investigate the elasto-plastic response.

An alternative to experiments is the simulation of the system using the discrete elements method (DEM), where the trajectory of individual grains is obtained by the calculation of the interaction forces between particles and integrating the equations of motion [1]. In the simplest case visco-elastic rules can be imposed at each contact, different for the normal and the tangential direction [7,8], but also plastic deformations, adhesion/cohesion and Coulomb friction are implemented in more advanced models.

In both experiments and simulations, the plastic behavior of powder samples depends on the applied strain and on the history of the material [9]. Under bi- or tri-axial deformation, the response of the system is characterized by elastic behavior for very small deformations, softening, plastic yield and critical state flow at large strain. When the original stress-state is restored, the structure of the system is in general different from the original: Hysteretic behavior is observed under repeated, cyclic loading and is, in fact, a very relevant characteristics of granular materials. The extensive use of non-cohesive, dry granular materials in foundations of buildings and as roadbeds indicates the urge for developing more efficient methods to understand the effects caused by quasi-static, possibly cyclic loading.

When materials accumulate strain in every cycle, their behavior is called ratcheting – if the strain accumulation stops after several cycles, the behavior is called shake-down. The concept of ratcheting was introduced in soil mechanics in order to describe the gradual accumulation of a small permanent deformation [6]. Ratcheting is however a much more general concept that has also been studied, driven by the need of understanding steel behavior [4] or biophysical systems such as molecular motors [3]. In a 2D granular packing of discs, subjected to stress controlled cyclic loading, strain accumulations were identified as shakedown, or ratcheting, depending on the amplitude of the stress variations. This particular phenomenon has been intensively investigated in 2D [2,5] and more recently also in 3D [10].

Since the accumulation of strain and the change of the structure is strongest in the first loading period, in this paper, rather than applying cyclic deformations with small strains, we focus on the first load period only but apply very large strain and compare directly 2D and 3D results against each other.

II. DEM MODEL

The elementary units of granular materials, the "mesoscopic" particles, deform locally under stress at the contact point. The realistic modeling of this deformation would be computationally very expensive. Thus the interaction force is related to the overlap of two particles. As a further simplification, these two particles interact only if they are in contact (short range forces), and the force between them is decomposed into a normal and a tangential part.

The *normal force* is, in the simplest case, a linear spring that takes care of repulsion, and a linear dashpot that accounts for dissipation during contact.

$$f_i^n = k\delta + \gamma_0 \dot{\delta}\,, \tag{1}$$

with spring constant k and some damping coefficient γ_0. The half period of a vibration around the equilibrium position can be computed, and one obtains a typical contact duration (response time) $t_c = \pi/\omega$, with $\omega = \sqrt{(k/m_{ij}) - \eta_0^2}$, the eigenfrequency of the contact, the reduced mass $m_{ij} = m_i m_j/(m_i + m_j)$, and the rescaled damping coefficient $\eta_0 = \gamma_0/(2m_{ij})$. The energy dissipation during a collision, as caused by the dashpot is quantified by the restitution coefficent $r = -v_n'/v_n = \exp(-\eta_0 t_c)$, where the prime denotes the normal velocity after a collision.

The *tangential force* involves dissipation due to Coulomb friction, but also some tangential elasticity that allows for stick-slip behavior on the contact level [7]. In the static case, the tangential force is coupled to the normal force, Eq. (1), via Coulomb's law, i.e. $f^t \le \mu_s f^n$, where for the limit sliding case one has the dynamic friction with $f^t = \mu_d f^n$. The dynamic and the static friction coefficients follow, in general, the relation $\mu_d \le \mu_s$. However, for the following simulations, we will apply $\mu = \mu_d = \mu_s$. The static case requires an elastic spring in order to allow for a restoring force, i.e., a non-zero remaining tangential force in static equilibrium due to activated Coulomb friction.

If a contact exists with non-zero normal force, the tangential force can be active too, and we project the corresponding tangential spring into the actual tangential plane. This is necessary, since the frame of reference of the contact may have slightly rotated since the last time-step. $\vec{\xi} = \vec{\xi}' - \hat{n}(\hat{n}\cdot\vec{\xi}')$, where $\vec{\xi}'$ is the old spring from the last iteration, and $\hat{n}$ is the normal unit vector. This action is relevant only for an already existing spring; if the spring is new, the tangential spring-length is zero, but its change is well defined for the next time-interval. The tangential velocity is $\vec{v}_t = \vec{v}_{ij} - \hat{n}(\hat{n}\cdot\vec{v}_{ij})$, with the total relative velocity of the contact surfaces of the particles (*i*,*j*):

$$\vec{v}_{ij} = \vec{v}_i - \vec{v}_j + a_i\,\hat{n}\times\vec{\omega}_i + a_j\,\hat{n}\times\vec{\omega}_j\ . \tag{2}$$

Next, we calculate the tangential test-force as the sum of the tangential spring and a tangential viscous force (in analogy to the normal viscous force):

$$\vec{f}_0^{\,t} = -k_t \vec{\xi} - \gamma_t \vec{v}_t \quad , \tag{3}$$

with the tangential spring stiffness k_t and a tangential dissipation parameter γ_t. As long as $\left|\vec{f}_0^{\,t}\right| \le f_C^s$, with $f_C^s = \mu_s f^n$, one has *static friction* and, on the other hand, if $\left|\vec{f}_0^{\,t}\right| > f_C^s$, sliding, *dynamic friction* becomes active, with $f_C^d = \mu_d f^n$. Sliding is active as long as $\left|\vec{f}_0^{\,t}\right| > \mu_d f^n$, and is changed to sticking only as soon as $\left|\vec{f}_0^{\,t}\right| \le f_C^d$ is reached. The corresponding states (static or dynamic) are kept in memory, to be used in the following time-step – and for contact statistics.

In the *static case*, the tangential spring is incremented, $\vec{\xi}' = \vec{\xi} + \vec{v}_t \Delta t_{MD}$, with the time step Δt_{MD} of the DEM simulation, to be used in the next iteration, and the tangential force, Eq. (3), is used.

In the latter, *sliding case*, the tangential spring is adjusted to a length, which is consistent with Coulombs condition

$$\vec{\xi}' = -(1/k_t)\left(f_C^d \hat{t} + \gamma_t \vec{v}_t\right) \quad , \tag{4}$$

with the tangential unit vector, $\hat{t} = \vec{f}_0^{\,t} \Big/ \left|\vec{f}_0^{\,t}\right|$, defined by the direction of the tangential test force above, and thus the magnitude of the sliding Coulomb force is used. Inserting the new spring length into Eq. (3) leads to $f_0^t \approx f_C^d$. Note that $\vec{f}_0^{\,t}$ and $\vec{v}_t$ are not necessarily parallel in three dimensions.

If all forces are known, acting on a selected particle (either from other particles, boundaries or external forces like gravity or a background damping $\vec{f}_i^{\,b} = -\gamma_b \vec{v}_i$), the problem is reduced to the integration of Newton's equations of motion for the translational and rotational degrees of freedom:

$$m_i \frac{\mathrm{d}^2}{\mathrm{d}t^2} \vec{r}_i = \vec{f}_i + m_i \vec{g} \quad \text{and} \quad I_i \frac{\mathrm{d}}{\mathrm{d}t} \vec{\omega}_i = \vec{t}_i \quad , \tag{5}$$

with the gravitational acceleration $\vec{g}$, the mass m_i of the particle, its position $\vec{r}_i$, the total force $\vec{f}_i = \sum_c \vec{f}_i^{\,c}$, acting on it due to contacts with other particles or with the walls, its moment of inertia I_i, its angular velocity $\vec{\omega}_i$, and the total torque $\vec{t}_i = \sum_c \vec{l}_i^{\,c} \times \vec{f}_i^{\,c}$, with the center-contact "branch" vector $\vec{l}_i^{\,c}$.

The DEM simulations consider both two- and three-dimensional bi- and tri-axial geometries, where the walls are either strain- or stress-controlled. For the initial preparation of the sample, the particles (with radii randomly drawn from a homogeneous distribution in 2D [7] and from a Gaussian distribution in 3D [10]) were initially arranged on a square lattice (big enough for them not to overlap) with rather large velocities in order to allow them to escape from the ordered structure. Then the box is compressed by imposing a confining pressure, p_0, in order to achieve a homogeneous, isotropic initial condition. Inhomogeneities in the distribution of large and small particles were observed when the compression was performed too fast and only from one side. The 3D simulations presented below were compressed from all sides at the same time to avoid this effect. The preparation stage is finished when the kinetic energy becomes much smaller than the potential energy stored in the contacts. A periodic, strain-controlled loading with period t_0 is then applied through a side of the box, while keeping the other stresses constant.

III. SIMULATION RESULTS

In order to compare the two- and three-dimensional DEM simulation, we first assure that the time step Δt_{MD} used for integration is small, so that $\Delta t_{\mathrm{MD}} << t_c < t_b < t_0$, where t_c is the typical duration of a contact interaction or vibration, t_b is the relaxation time scale due to dissipation, and t_0 is the period of the applied strain. Second, we will compare dimensionless quantities like strain and stress (rescaled by the constant confining stress p). For examples of the model system, see Fig. 1 for a snapshot of typical systems in 2D and 3D.

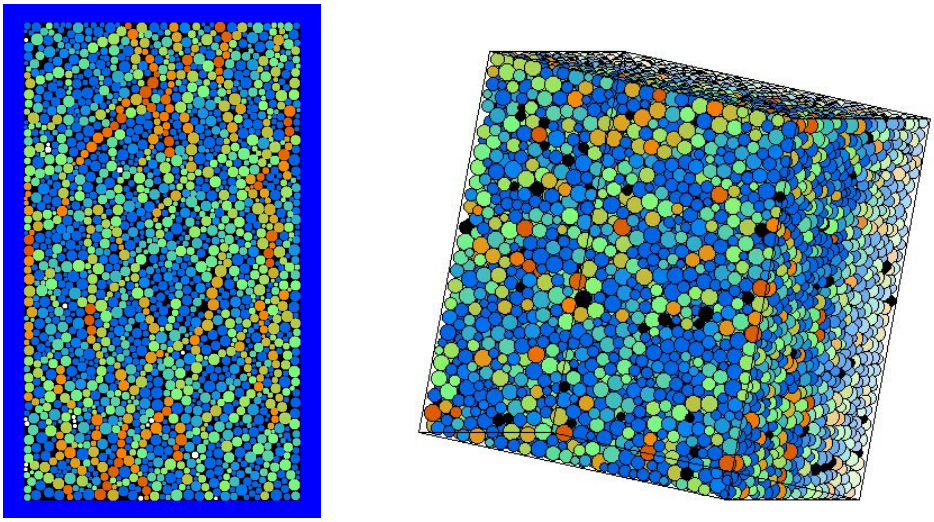

Figure 1: Snapshot of the model systems in 2D (left) with N=1950 particles, see [7,8] for details, and in 3D (right) with N=20000 particles. The color code blue/green/red indicates particles feeling weak/medium/strong forces.

Deformations can be applied directly, by controlling strain, or indirectly by controlling/varying stress. The former approach was used in Refs. [7,8] for 2D samples, the latter for the 3D cyclic loading case [10]. Here, the old 2D results [7,8] are compared to new 3D data with a strain-controlled compression in one direction and a constant stress, $p = \sigma_{zz} = \sigma_{yy}$, in the other direction(s). The strain and stress are split in their volumetric (isotropic) and deviatoric components indicated by the subscripts V and D, respectively. For the stress in 2D, we use $\sigma_V = \left(\sigma_{xx} + \sigma_{yy}\right)/2 \cong \left(\sigma_{xx} + p\right)/2$ and $\sigma_D = \left(\sigma_{xx} - \sigma_{yy}\right)/2 \cong \left(\sigma_{xx} - p\right)/2$; the stresses in 3D are $\sigma_V = \left(\sigma_{xx} + \sigma_{yy} + \sigma_{zz}\right)/3 \cong \left(\sigma_{xx} + 2p\right)/3$ and $\sigma_D = \left(2\sigma_{xx} - \left(\sigma_{yy} + \sigma_{zz}\right)\right)/3 \cong 2\left(\sigma_{xx} - p\right)/3$. An equivalent definition is used for the deviatoric strain ε_D, based on the deformation of the volume in the three directions. The volumetric strain is defined as $\varepsilon_V = V/V_0 - 1$, where V is the volume of the sample and the subscript 0 indicates the value at the beginning of the test. The volumetric strain based on the trace of the strain tensor is identical to the volume-based definition for small deformations. Simulations with slower deformation and with larger systems are in progress and will be presented elsewhere. The simulation parameters are described in more detail in Refs. [7,8,10] – the coefficient of friction $\mu = 0.5$ is the same in 2D and 3D, but the particle number is N=1950 and N=1728 in 2D and 3D, respectively. Some of the differences in the packings (2D/3D geometry and aspect ratio, system-size, particle size distribution, and preparation procedure) are likely to have an effect on the packing and on the behavior as presented below – a better understanding of this is also work in progress. The 3D system is comparable in particle number but considerably smaller concerning system size measured in particle diameters – system size dependence of the present results needs further investigation [10].

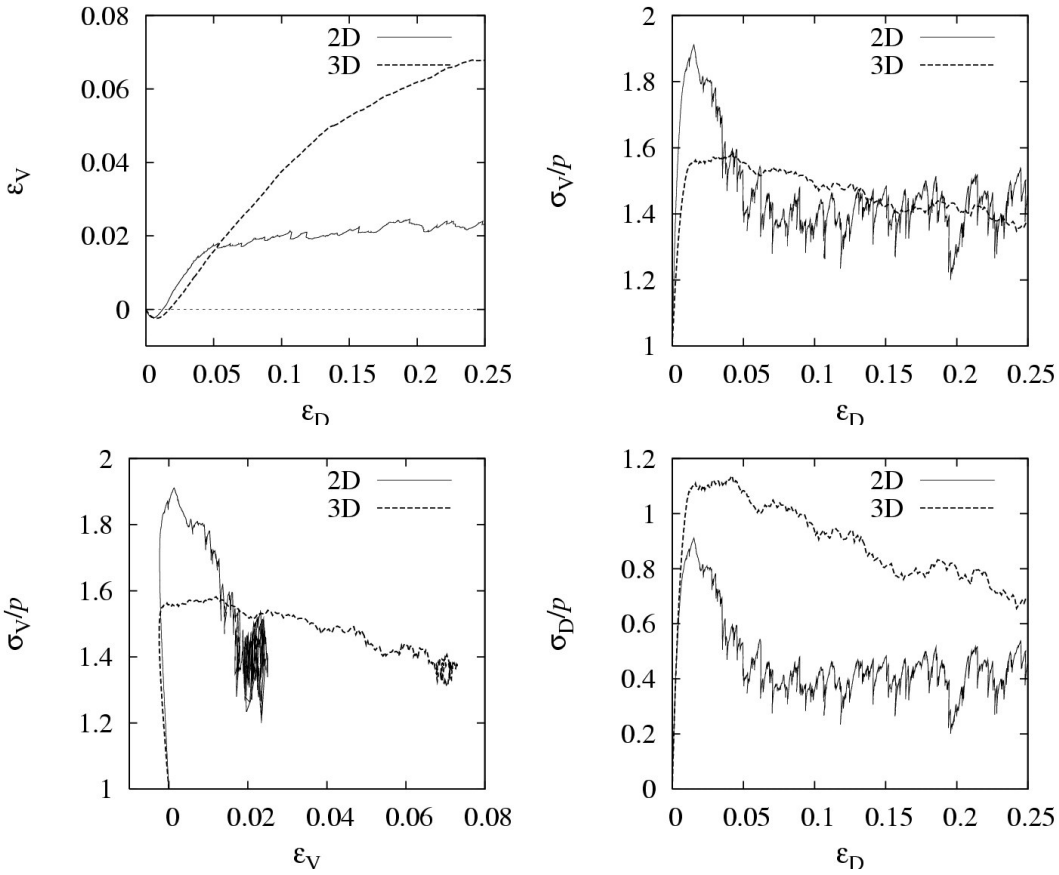

Figure 2: Stress and strain relations in the model systems, where the solid and dashed lines are 2D and 3D results, respectively: (top left) volumetric strain plotted against deviatoric strain – negative values mean compression, positive values dilation; (top right) scaled isotropic stress plotted against deviatoric strain and (bottom left) plotted against volumetric strain; (bottom right) deviatoric stress plotted against deviatoric strain.

In Fig. 2 the stresses and strains are plotted in various combinations. The volumetric strain first decreases (compression) and then increases (dilation) until it reaches a saturation level (critical state flow). While the compression level and the rate of dilation are comparable in 2D and 3D, the saturation level is much higher and reached at much larger deformations (about 25%) in the 3D system, i.e., the 3D system is more dilatant than its 2D counterpart and also needs more strain to reach the critical state regime. The stress-strain relations consist of an initial, linear elastic part starting from the origin – for very small deformations. In this regime 2D and 3D behave qualitatively similarly, the scaled deviatoric stress is almost in quantitative agreement (data not shown here). At increasing deformation the stress reaches a maximum and decreases down to the critical state flow level. The stress decrease appears rapid in 2D and rather smooth and slow in 3D, the peak isotropic stress is larger in 2D than 3D while the peak deviatoric stress is smaller in 2D than in 3D. The critical state level of the isotropic stress is comparable in 2D and 3D while the deviatoric critical state stress level is slightly larger in 3D. Finally, the stress fluctuations appear much stronger in 2D than in 3D even though the particle number is comparable in both samples.

IV. SUMMARY AND CONCLUSIONS

In summary, quasi-static bi- and tri-axial deformation of frictional powders show an elastic regime, a yield-stress, and critical state flow in both 2D and 3D simulations. Shakedown and ratcheting

after many cycles of load were observed previously in 2D and 3D model granulates, both consisting of polydisperse, frictional spheres [10]. The present results indicate qualitative differences between 2D and 3D systems. The critical state regime is reached at larger deformation and at a considerably higher dilation level in 3D. Reasons for the differences can be the system size, the geometry and the aspect-ratio as well as different definitions of stress and strain in different dimensions, and the coordination numbers and the porosity/density are very different in 2D and 3D. Smaller systems have more particles that are in contact with the wall and in systems with different aspect ratio, shearbands can be influenced differently by the corners. Furthermore, the size distribution could be responsible, this is unlikely in our opinion as long as the distribution is wide enough to avoid crystallization effects. The geometry and local structure are different in 2D and in 3D due to the additional degree of freedom, which could lead to different behavior given that material parameters like friction are identical. The last possible reason for the systems to behave differently is the preparation procedure. This could not be objectively controlled and tuned, so that an overconsolidation in 2D and a critical consolidation in 3D can partially explain the slow softening in 3D.

Thus, the present study is only the first step towards a more detailed exploration of the influence of various other material- and system-parameters, involving variations of the strain and stress amplitudes, of the friction model, boundary conditions, and others. Comparison with experiments for validation is the next natural step towards the better understanding of the quasi-static deformation of frictional powder systems.

V. ACKNOWLEDGEMENTS

The authors acknowledge support from the EU project Degradation and Instabilities of Geomaterials with Application to Hazard Mitigation (DIGA) in the framework of the Human Potential Program, Research Training Networks (HPRN-CT-2002-00220), from the Deutsche Forschungsgemeinschaft (DFG), and from FOM (Fundamenteel Onderzoek der Materie), financially supported by the Nederlandse Organisatie voor Wetenschappelijk Onderzoek (NWO).

VI. REFERENCES

[1] Allen, M., P. Tildesley (1987). *Computer Simulation of Liquids.* Oxford: Oxford University Press.

[2] Alonso-Marroquin F. and H. J. Herrmann (2004). *Ratcheting of granular materials*, Phys. Rev. Lett. 92, 054301 (2004).

[3] Astumian, R. (2001). *Making molecules into motors*, Scientific American 58, 57–64.

[4] Colak, O. U. and E. Krempl (2003). *Modelling of uniaxial and biaxial ratcheting behavior of 1026 Carbon steel using the simplified Viscoplasticity Theory Based on Overstress*, Acta Mechanica (New York) 160, 27–44.

[5] García-Rojo, R. and H. J. Herrmann (2005). *Shakedown of unbound granular material*, Granular Matter 7(2-3), 109–118.

[6] Lekarp, F., U. Isacsson and Dawson A (2000). *Permanent strain response of unbound aggregates*, J. Transp. Engng.-ASCE 126 (1). 66–83.

[7] Luding, S. (2004), *Micro-macro transition for anisotropic, frictional granular packings*. Int. J. Sol. Struct. 41, 5821–5836.

[8] Luding S. (2004), *Molecular dynamics simulations of granular materials*. In H. Hinrichsen and D. E. Wolf (Eds.), The Physics of Granular Media, Wiley VCH, Weinheim, Germany, pp 299–324.

[9] Vanel, L., D. Howell, D. Clark, R.P. Behringer and E. Clement (1999), *Memories in Sand: Experimental tests of construction history on stress distributions under sandpiles*, Phys. Rev. E 60 (5), R5040-R5043.

[10] David, C. T., R. Garcia Rojo, H. J. Herrmann, and S. Luding, (2005) *Hysteresis and creep in powders and grains* , in: Powders and Grains 2005, Stuttgart, July 2005, R. Garcia-Rojo, H. J. Herrmann, and S. McNamara (Eds.), Balkema, Leiden, Netherlands, pp. 291–294.

[11] J. Schwedes (2004) *Review on testers for measuring flow properties of bulk solids (based on an IFPRI-Report 1999)*, Granular Matter 5(1), 1–43

[12] Janssen, R., and M. Verwijs (2006) *Why does the world need a true triaxial tester?* printed in this special issue.

[13] M. Verwijs (2006) *Powder Flow: The 4M Business and Systems Approach*, printed in this special issue.